Evaluation of Catalyst Deactivation during Catalytic Steam Reforming of Biomass-Derived Syngas

Richard L. Bain,* David C. Dayton, Daniel L. Carpenter, Stefan R. Czernik, Calvin J. Feik, Richard J. French, Kimberly A. Magrini-Bair, and Steven D. Phillips

National Renewable Energy Laboratory, 1617 Cole Boulevard, Golden, Colorado 80401

Mitigation of tars produced during biomass gasification continues to be a technical barrier to developing systems. This effort combined the measurement of tar-reforming catalyst deactivation kinetics and the production of syngas in a pilot-scale biomass gasification system at a single steady-state condition with mixed woods, producing a gas with an H_2-to-CO ratio of 2 and 13% methane. A slipstream from this process was introduced into a bench-scale 5.25 cm diameter fluidized-bed catalyst reactor charged with an alkali-promoted Ni-based/Al_2O_3 catalyst. Catalyst conversion tests were performed at a constant space time and five temperatures from 775 to 875 °C. The initial catalyst-reforming activity for all measured components (benzene, toluene, naphthalene, and total tars) except light hydrocarbons was 100%. The residual steady-state conversion of tar ranged from 96.6% at 875 °C to 70.5% at 775 °C. Residual steady-state conversions at 875 °C for benzene and methane were 81% and 32%, respectively. Catalytic deactivation models with residual activity were developed and evaluated based on experimentally measured changes in conversion efficiencies as a function of time on stream for the catalytic reforming of tars, benzene, methane, and ethane. Both first- and second-order models were evaluated for the reforming reaction and for catalyst deactivation. Comparison of experimental and modeling results showed that the reforming reactions were adequately modeled by either first-order or second-order global kinetic expressions. However, second-order kinetics resulted in negative activation energies for deactivation. Activation energies were determined for first-order reforming reactions and catalyst deactivation. For reforming, the representative activation energies were 32 kJ/g·mol for ethane, 19 kJ/g·mol for tars, 45 kJ/g·mol for tars plus benzene, and 8−9 kJ/g·mol for benzene and toluene. For catalyst deactivation, representative activation energies were 146 kJ/g·mol for ethane, 121 kJ/g·mol for tars plus benzene, 74 kJ/g·mol for benzene, and 19 kJ/g·mol for total tars. Methane was also modeled by a second-order reaction, with an activation energy of 18.6 kJ/g·mol and a catalyst deactivation energy of 5.8 kJ/g·mol.

Introduction

The mitigation of tars produced during biomass gasification continues to be a challenge for developing thermochemical conversion processes. Strict gas cleanup requirements have been established for downstream syngas utilization for power generation, fuel synthesis, and hydrogen production. The goals of this study were to investigate the initial deactivation kinetics of reforming catalysts applied to the conversion of high-molecular-weight hydrocarbons, tars, present in the product gas generated in a pilot-scale biomass gasification system. A single steady-state process condition was established for the steam gasification of a mixed hard and soft wood fuel producing a gas with an H_2-to-CO ratio of 2 and 13% methane. A slipstream from this process was introduced into a bench-scale, 5.25 cm (2 in.) diameter fluidized-bed reactor charged with an Ni-based/Al_2O_3 catalyst. Catalyst deactivation tests and steady-state activity measurements were performed at a constant space time and five temperatures from 775 to 875 °C. The catalyst being tested was the culmination of several years' effort to develop a fluidizable reforming catalyst for the production of H_2 from various feedstocks [1,2] and the destruction of biomass gasification tars. Comprehensive gas analysis—before and after the catalyst reactor—permitted a detailed kinetic evaluation of tar reforming and catalyst deactivation.

Biomass gasification is a complex thermochemical process that consists of a number of elementary chemical reactions that begin with the partial oxidation of a lignocellulosic fuel with a gasifying agent, usually air, oxygen, or steam. Volatile matter that is released as the biomass fuel is heated partially oxidizes to yield the combustion products H_2O and CO_2, plus heat to continue the endothermic gasification process. Water vaporizes and biomass pyrolysis continues as the fuel is heated. Thermal decomposition and partial oxidation of the pyrolysis vapors occurs at higher temperatures to yield a product gas composed of CO, CO_2, H_2O, H_2, CH_4, other gaseous hydrocarbons, tars, char, inorganic constituents, and ash. The actual biomass gasification product gas composition depends heavily on the gasification process, the gasifying agent, and the feedstock composition.[3−5]

Gas conditioning is a general term for removing the unwanted impurities from gasification product gas and generally involves an integrated, multistep approach that depends on the end use of the product gas. The inorganic impurities such as sulfur species, chlorides, nitrogen species (NH_3 and HCN), and alkali metals are typically poisons for downstream catalytic synthesis processes and yield unwanted emissions from downstream prime movers. Fixed bed sorbents can usually

* To whom correspondence should be addressed. E-mail: richard_bain@nrel.gov.

10.1021/ie050098w CCC: $30.25
Published on Web 09/17/2005

reduce these impurities to acceptable levels. The organic impurities range from low-molecular-weight hydrocarbons to high-molecular-weight polynuclear aromatic hydrocarbons. The lower-molecular-weight hydrocarbons can be considered as fuel in gas turbine or engine applications but are undesirable products in fuel synthesis processes. The higher-molecular-weight hydrocarbons are collectively known as "tar".

Optimizing gasification processes by thermally integrating the gasifier with downstream gas conditioning operations maximizes thermodynamic efficiency. Hot gas conditioning eliminates tars by converting them into desired product gas components via catalytic steam reforming, thus retaining their chemical energy in the product gas. Numerous catalysts have been tested for tar destruction activity at a broad range of scales. Recent literature[6,7] summarizes catalytic biomass gasification tar destruction and provides an overview of the different catalysts that have been studied and how they have been implemented. Catalytic tar destruction has been studied for several decades and a number of reviews have been written on biomass gasification hot gas cleanup.[8,9]

Calcined dolomites are the most widely used nonmetallic catalysts for tar conversion in biomass gasification processes.[10−16] They are relatively inexpensive and are considered disposable; however, they quickly undergo attrition in fluidized-bed reactors. Tar-conversion efficiency is high when calcined dolomites are operated at high temperatures (900 °C) with steam. Olivine, another naturally occurring mineral, has also demonstrated tar-conversion activity similar to that of calcined dolomite. Olivine has been shown to resist attrition better than calcined dolomite and has been applied as a primary catalyst to reduce the output tar levels from fluidized-bed biomass gasifiers.[15,17−19]

Commercial Ni steam-reforming catalysts have also been used for biomass gasification tar conversion, usually as secondary catalysts in separate fixed or fluidized-bed reactors operated independently to optimize performance.[20−26] They have high tar-destruction activity with the added advantages of completely reforming methane and having water gas shift activity to adjust the H_2-to-CO ratio of the product gas. Corella et al.[27] tested seven commercial catalysts for upgrading of biomass gasification product gas. All of the catalysts were Ni-based catalysts with varying amounts of Mg, Ca, and K and multiple supports (Al_2O_3, SiO_2, and $MgAl_2O_4$). They reported on changes in global gas composition with the formation and destruction of methane. They reported that naphtha catalysts had a higher reforming activity than did steam−methane-reforming catalysts. Some studies have also shown that nickel catalyzes the reverse ammonia reaction, thus reducing the amount of NH_3 in the gasification product gas.[28−30]

A limitation of using nickel catalysts for hot gas conditioning of biomass gasification product gases is rapid deactivation, leading to limited catalyst lifetimes. Corella et al. compared the effectiveness of commercial steam-reforming catalysts, commercial methanation catalysts, and naturally occurring minerals (dolomites, calcites, and magnesites) for tar reforming. They reported tar conversions of 95−99.99% at initial activity, followed by rapid deactivation to some lower residual activity.[31]

Nickel catalyst deactivation is caused by several factors. Sulfur, chlorine, and alkali metals that may be present in gasification product gases act as catalyst poisons and cause irreversible loss of catalytic activity.[32−35] A reaction that competes with the steam reforming of tars is the formation of carbon deposits, or coke, on the active catalyst sites. Studies investigating steam reforming of model tar compounds over metallic catalysts have been conducted to investigate the specific chemical mechanisms that describe tar reforming and catalyst deactivation from surface carbon deposition (coke formation). This work can be used to help optimize catalyst formulations and process conditions for the specific compound of interest.[36−41] Any matrix effects from the presence of other tar compounds in biomass-derived syngas, however, are clearly not accounted for.

Coke formation on the catalyst surface can be substantial in fixed-bed reactors when tar levels in product gases are high, eventually leading to a prohibitively large pressure drop at the inlet. Coke can be removed by regenerating the catalyst, and activity can usually be restored. However, repeated high-temperature processing of nickel catalysts can lead to sintering, phase transformations, and volatilization of the nickel. A review of sintering for conventional supported metal catalysts was presented by Bartholomew.[42] Included was the application of a generalized power law expression to reanalyze available experimental data. He showed that all of the available dispersion-versus-time data could be fitted by either first- or second-order kinetics. He presented activation energies for Ni/γ-Al_2O_3 in hydrogen between 773 and 1073 K ranging from 31 to 159 kJ/g·mol.

Fluidization can be utilized to optimize the contact between catalyst and tars, maximizing activity and ensuring that catalyst particles with surface coke deposits are evenly distributed in the reactor. Mleczko and Wurzel[43] experimentally investigated a dual fluid-bed reformer−combustor for the CO_2 reforming of methane. The heat needed for CO_2 reforming was generated by the catalytic combustion of methane over a reforming catalyst and the heat transferred to the reformer by hot particles. A Ni (1 wt %)/ α-Al_2O_3 catalyst was found to be active not only for the reforming reaction but also for the combustion of methane. The experiments confirmed that catalyst activity, which decreased during reforming, could be restored in the combustor.

Steam reforming of biomass-derived vapors and tars has been a primary research focus at the National Renewable Energy Laboratory (NREL) for several years.[1,2,44] This study and previous studies have integrated the production of raw, biomass-derived syngas in NREL's Thermochemical Process Development Unit, a bench-scale fluidized-bed tar-reforming reactor, and comprehensive gas analysis at the inlet and outlet of the reforming reactor to evaluate the tar-reforming activity and lifetime of various commercial and novel catalysts. The ultimate goal of catalyst screening is to determine the initial catalyst deactivation kinetics for methane, other light hydrocarbons, benzene, and total tar reforming.

Pioneering work in this area was performed by Mudge and co-workers in the 1970s and 1980s.[45−49] Corella and co-workers have described similar efforts using a biomass gasification pilot plant to study catalytic product gas conditioning of both slipstreams and full gasifier output.[5,20,21] Their approach was to use an initial fixed dolomite guard bed upstream from a fixed-bed Ni

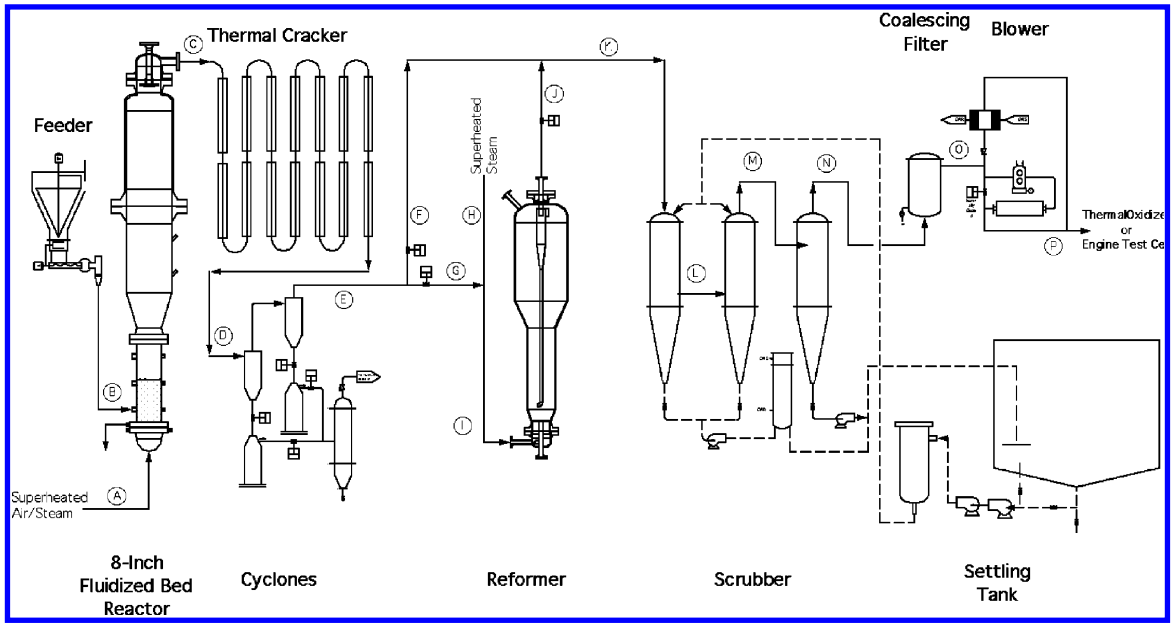

Figure 1. Process flow sheet for the Thermochemical Process Development Unit (TCPDU).

catalyst reactor. They determined effective kinetic parameters by fitting their results to a model that categorized tars in different "lumps" based on the chemical composition of the tars.[50−53] One kinetic model evaluated is based on tar as a continuous mixture of different species that is described by a specific molecular-weight distribution. Catalyst deactivation corresponds to an increase in product gas molecular weight with time. A second kinetic model is based on six lumps to describe the tar. The number of aromatic rings in the tar species defines the lumps. These kinetic models describe the complex process of catalytic tar destruction in a global sense, with additional levels of detail added by how the global description is divided into smaller subsystems based on compound classes.

Experimental Methods

A slipstream from a biomass steam gasification process development unit with a maximum capacity of 0.6 ton/day was delivered to a bench-scale fluidized-bed steam-reforming reactor loaded with a fluidizable nickel-based reforming catalyst. Comprehensive, real-time gas-composition analysis at the inlet and outlet of the catalyst reactor provided quantitative measurement of the decay of hydrocarbon conversion with time over the catalyst. In concert, these integrated experimental facilities provide an opportunity for ultimately developing a mechanistic description of tar reforming with the level of detail previously obtained in model compound studies while also exploring the potential matrix effects induced by the suite of hydrocarbons and impurities present in the biomass gasification product gases. This detailed description can then be condensed into a more global description of biomass gasification tar reforming that can be incorporated into reactor designs and process engineering models for developing commercial-scale systems.

Thermochemical Process Development Unit (TCPDU). The TCPDU is an electrically heated integrated system of unit operations combined to investigate various aspects of biomass thermochemical conversion to gaseous and liquid fuels and chemicals.

Table 1. Proximate and Ultimate Analysis for the Wood Feed Stock Used during Gasification

proximate analysis (wt. %) as received	
moisture	3.74
ash	0.63
volatiles	82.68
fixed carbon	12.95
higher heating value (MJ/kg)	18.78

ultimate analysis (wt. %) as received	
moisture	3.74
carbon	51.36
hydrogen	6.25
nitrogen	0.11
sulfur	0.02
ash	0.63
oxygen	37.89

elemental analysis (wt. %) as received			
SiO_2	0.17	Na_2O	0.01
Al_2O_3	0.04	K_2O	0.09
TiO_2	<0.01	P_2O_5	0.02
Fe_2O_3	0.02	SO_3	<0.01
CaO	0.14	Cl	<0.01
MgO	0.03	CO_2	0.10

A process flow diagram of the TCPDU is shown in Figure 1. The feeding system consists of a loss-in-weight feeder with a 0.450 m^3 hopper (200 kg capacity). Pelletized biomass is metered into a crusher that grinds the material to −2.3 mm particle size. The material passes through a pair of rotary valves that isolate the process from the feeding system and onto a 22 mm diameter screw which augers the feed into the gasifier at a rate of between 5 and 25 kg/hr. The feedstock used for the tar-reforming experiments was a pelletized mixture of hard and soft woods (15% white pine, 25% red oak, 15% maple, 15% ash, 10% poplar, and 20% cherry−birch−cedar) provided by New England Wood Pellet, Inc. of Jaffrey, New Hampshire. Comprehensive fuel analyses are reported in Table 1.

The first and primary reactor in the process is a 20.3 cm (8 in.) diameter fluidized-bed reactor with a 40.6 cm (16 in.) diameter freeboard. The bed zone is 76.6 cm (34 in.) high. The freeboard zone is 170.2 cm (67 in.) high connected by a 29.2 cm (11.5 in.) high frustrum. The total rector volume is 0.26 m^3 (9.10 ft^3)

after accounting for the volume displaced by the sand used in the bed. Silica sand (16 kg) was used as the bed media. Over the range of possible gasifier operation, 5−25 kg h^{-1}, the feed mass velocity was 154−772 kg $h^{-1}m^{-2}$. The bubbling bed was fluidized with superheated steam for these gasification experiments. The minimum steam flow to maintain fluidization of silica sand (177−297 μm) bed material is 10 kg h^{-1} (gasifier mass velocity of 309 kg h^{-1} m^{-2}) to maintain a superficial gas velocity of 25 cm/s (0.8 ft/s). Typical steam flow rates are varied between 10 and 30 kg/hr, depending on biomass feed rate and desired gas composition. The maximum attainable bed temperature for these conditions is 725 °C.

Gas and entrained char and bed material flows out of the fluidized-bed reactor through a 3.81 cm (1.5 in.) diameter pipe into a thermal cracker. The thermal cracker is a 26 m (85 ft) long by 3.81 cm (1.5 in.) diameter tubular reactor with 11 independently controlled, electrically heated zones used to raise the product gas temperature to a maximum of 950 °C. Thermal conditioning of the tars and adjustment of the product gas composition from additional water gas shift occurs in this process step. The volume of the thermal cracker is ~0.028 m^3 (1.0 ft^3).

The product gas temperature is reduced to 450°C prior to entering two cyclone separators in series with 10.2 cm (4 in.) and 7.6 cm (3 in.) diameter barrels, respectively. The solids removed in these cyclones are collected in char pots below the cyclones. The char pots are emptied periodically into an intermediate vessel where the char is cooled using nitrogen gas. The cooling vessel is operated like a lock hopper. Once the char has cooled, it is transferred from the intermediate vessel into a bag for further analysis or disposal.

The gas leaving the cyclones moves quickly through the remaining 3.81 cm (1.5 in.) diameter pipe to the condensation system. The volume of the piping between the cyclones and the condensation system is ~0.007 m^3 (0.25 ft^3). Heated sample ports are available in this section of the process for removing hot product gases or vapors and directing them to on-line analytical equipment for compositional analysis.

The condensation operation consists of two 25.4 cm (10 in.) diameter vessels connected sequentially with nozzles in the top to spray in cooling liquid. The liquid flow rate is ~0.114 m^3/min (30 gpm). This is sufficiently high to keep the cooling liquid from heating significantly as it contacts the hot gases and vapors entering the condensation vessels. A heat exchanger is available to remove heat from the cooling liquid if needed. Typically, water is used as the cooling liquid.

A knock out vessel with a pleated cartridge filter is located after the scrubber vessels to remove any remaining particulate matter. The knock out vessel also serves as a buffer between the condensation operation and the downstream unit operations.

Filters (2 μm) remove entrained particles or droplets exiting the knockout vessel. Difficult-to-remove aerosols are also removed at this point. Typically, an insignificant quantity of liquid is removed from this vessel during gasification operation. These filters also serve as a guard for the positive-displacement (Roots-type) blower at the end of the process that boosts the process gas pressure to ~68.9 kPag (10 psig). Unless the process gas is to be used for some other purpose, it is sent to a thermal oxidizer where it is combusted at 650 °C.

Extensive analytical instrumentation is available for determining gas composition at the exit of the scrubbing system. With steam and other condensable vapors removed from the product gas stream, compositions can be measured with three on-line, continuous, nondispersive infrared (NDIR) chemical analyzers to monitor CO, CO_2, and CH_4; a thermal conductivity H_2 analyzer; a paramagnetic O_2 analyzer; a four-channel, rapid-analysis gas chromatograph that cycles every 2 min for measuring permanent gases and hydrocarbons up to C4; and a transportable molecular-beam mass spectrometer (TMBMS) for continuous, real-time monitoring of all gas-phase products with particular emphasis on tars and heteroatom products.

5.25 cm FBR Catalyst Reactor. The second integrated experimental component used in these studies was a 5.25 cm (2 in.) inner-diameter fluidized-bed reactor (2FBR). This bench-scale system, shown schematically in Figure 2, is used to investigate various thermal and catalytic processes such as pyrolysis, partial oxidation, and catalytic cracking/reforming for a variety of solid, liquid, and gaseous feedstocks. The configuration used for these experiments consists of an inconel, tubular, bubbling fluidized-bed reactor externally heated by a three-zone electric furnace up to 900 °C. Nitrogen at 4 standard liters per minute (slm) was used as the fluidizing gas. A slipstream of product gas from the TCPDU was metered through a heated transfer line and filter directly into the fluid-bed reformer through a 0.64 cm ($^1/_4$ in.) inconel sparger. The sparger was inserted through a side port located 1.91 cm ($^3/_4$ in.) above the distributor plate.

A nondispersive infrared analyzer (NDIR model 300 from California Analytical Instruments) continuously monitored CO_2, CO, and CH_4 concentrations in the reforming gas; and a thermal conductivity monitor (TCM4 from Gerhard Wagner, Germany) monitored hydrogen concentration. In addition, the gas is analyzed every 5 min by an on-line gas chromatograph, to measure hydrogen, carbon monoxide, carbon dioxide, methane, ethylene, and nitrogen concentration as a function of time.

Fluidizable Reforming Catalyst. The catalyst tested was the culmination of several years' effort to develop a robust, fluidizable reforming catalyst.[1,2,54,55] While the specific catalyst formulation used in this study is considered confidential for intellectual property reasons, a general discussion is given below. Industrial, packed-bed, reforming catalysts contain ~25 wt % NiO and 5−10 wt % K_2O on alumina supports. The catalyst formulation used for these studies is based on that of naphtha-reforming catalysts used to process heavy crude oils and residuals. Numerous support-screening experiments showed that commercially available specialty aluminas produced by CoorsTek Ceramics had the necessary strength to withstand fluidizing conditions (consistent losses <0.5 wt %/day). The best of the initial support materials, alpha alumina particles of 90−99% purity and 425−500 μm size, was used to prepare numerous Ni-based catalysts. The best catalyst compositions were modeled on commercial catalysts developed for reforming moderately heavy petroleum fractions. These materials contained ~0.1 wt % MgO (to stabilize Ni crystallite size), 2.0 wt % NiO, and 0.2 wt % K_2O (to promote surface gasification).

All catalysts were prepared by adding aqueous solutions of Ni, Mg, and K nitrate salts to the alumina

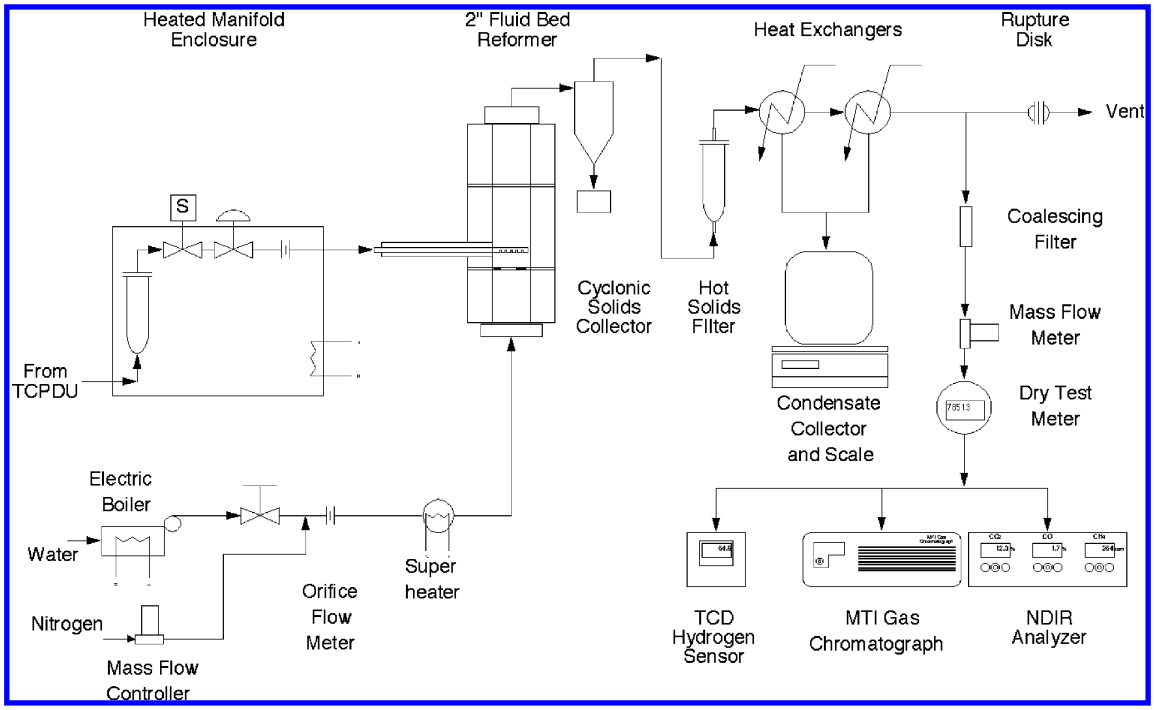

Figure 2. Schematic of the fluid-bed catalytic conversion system.

supports to incipient wetness. The catalysts were calcined at 650 °C in air to convert the metal salts to oxides, which were converted to active metals by hydrogen reduction at reaction temperatures prior to use. Subsequent performance tests evaluated catalyst activity for tar cracking and quantified attrition losses from extended use. The Ni−alumina catalyst, which exhibited minimal attrition, nearly matched the performance of the best commercial catalyst (Sud Chemie C 11 NK) while containing substantially less Ni and surface area.

Transportable Molecular Beam Mass Spectrometer (TMBMS). A transportable molecular-beam mass spectrometer (TMBMS) was used to provide continuous, on-line chemical analysis of hot process vapors at the inlet and outlet of the 2FBR. The hot gases exiting the process arrive at the entrance of the instrument by means of a heated sampling system. A molecular beam forms as the gases are extracted through a 300-μm orifice into a three-stage, differentially pumped vacuum system. The gases undergo a free-jet expansion, essentially halting chemical reactions and preventing condensation. Components of the molecular beam are then ionized by 22.5 eV electrons before passing through a quadrupole mass analyzer. The ions are then detected with an off-axis electron multiplier. This analytical technique has been used in previous laboratory investigations of a variety of high temperature, biomass thermochemical conversion process.[56−59]

Mass spectra were recorded for $m/z = 3-350$ along with data from the auxiliary channels at the rate of 5 scans/min. The temperatures of the raw gas sample lines and the orifice were all maintained at 450 ± 1 °C. The reformed gas sample lines were maintained at 350 ± 1 °C. The pressure in the sample line was also controlled, providing a constant flow to the orifice. As an internal measure of instrument stability, argon was introduced into the sampling system at a rate of 40 standard cc/min (sccm). In addition, two liquid calibration standards containing benzene, toluene, cresol, naphthalene, and phenanthrene were periodically injected into the sample line through a heated port downstream of the shut-off valves so that vapor-phase concentrations of those tar species could be quantified. The standard was injected off-line and diluted with a suitable flow of N_2 to simulate on-line pressures flow conditions

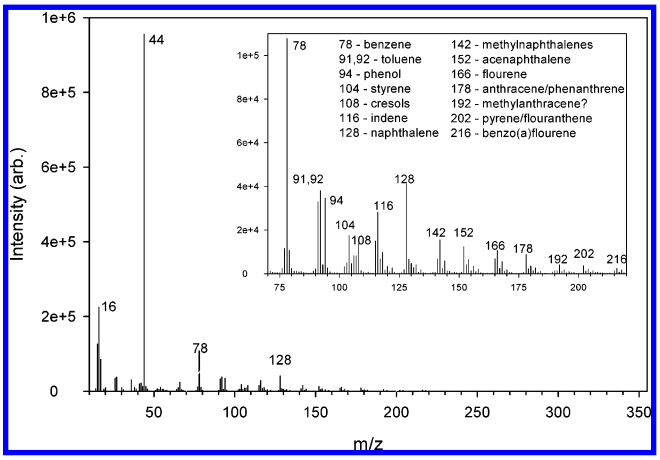

Figure 3. Typical averaged mass spectrum of products from indirect wood gasification as measured by TMBMS.

The raw gas produced in the TCPDU contained the typical slate of compounds found during wood gasification, including several tar species. The term "tars" is defined here as all aromatic hydrocarbons with a molecular weight >78.[58,59] A typical mass spectrum of the gasification products, taken with the TMBMS, is shown in Figure 3. As can be seen, the spectrum is dominated by $m/z = 44$ (CO_2), followed by $m/z = 16$ (methane). Carbon monoxide ($m/z = 28$) was not monitored since it could not be distinguished from N_2, also at $m/z = 28$, and would have saturated the detector. The insert shows several tar species on a magnified scale. Some other higher-molecular-weight hydrocarbon species were also seen up through $m/z = 300$. Acetylene, a known soot precursor, can be seen at $m/z = 26$ and was present in concentrations of ~0.1% in the wet gas.

Table 2. Representative Test Summary

conditions	
fluid bed temperature, °C	615 ± 3
thermal cracker temperature, °C	775 ± 2
biomass rate, kg/h	10.0 ± 0.4
steam rate, kg/h	20.0 ± 0.5
material balance (catalyst test period, exp. 042904)	
in (N_2 free)	
steam, kg	56.4
biomass, kg	27.9
total	84.3
out	
char, kg	1.9
condensables, kg	59.7
total gas, kg	25.2
N_2 in gas, kg	2.6
total (N_2 free)	84.2

Table 3. Average Dry Gas Composition

component	vol %
hydrogen	31.56 ± 0.96
carbon monoxide	15.40 ± 0.77
carbon dioxide	26.68 ± 0.77
methane	12.34 ± 0.29
acetylene	0.22 ± 0.03
ethane	0.54 ± 0.03
ethylene	2.39 ± 0.03
propane	nd[a]
propylene	0.29 ± 0.19
cis-2-butene	nd
trans-2-butene	nd
1-butene	0.1482 ± 0.0004
benzene	0.1164 ± 0.0109
toluene	0.0666 ± 0.0068
naphthalene	0.0219 ± 0.0015
other tars	0.2361 ± 0.0226
nitrogen	9.18 ± 1.24
helium	0.81 ± 0.03
total	100.00

[a] No data is denoted by nd.

Experimental Results

Table 2 presents a representative test summary. Gasification experiments were performed with the fluid-bed pyrolyzer at 615 °C and the thermal cracker at 775 °C at a biomass feed rate of 10 kg/h and a steam/biomass mass ratio of 2. Data were recorded in 1 min intervals. Since all process streams (with one exception) were measured in to and out of the TCPDU continuously in real time, mass closure could be calculated for any specified time period. Mass rates or total weight measurements were taken for all major inlet and outlet streams in addition to the accumulation in the scrubber settling tank. However, nitrogen used for purges and as a pressure seal in the feeding system was not measured directly, but it was measured at the outlet with the GC. The mass flow rate of the exit stream was then converted to exit mass flow rate on a nitrogen-free basis. The data were later reduced using common computer software to calculate the averages and standard deviations of all I/O points. Where intervals (±) are given, a 95% confidence level was used. For the number of measurements taken, this is essentially plus or minus twice the standard deviation. For the experiment shown, the overall material balance was 99.9%. Table 3 presents the average dry-gas composition from the TCPDU for all the tests in the study and represents a composite of gas chromatograph data and MBMS data.

Table 4. Reformer Gas Compositions[a] (Dry, Inert Gas-Free Basis)

temp (°C)	H_2	CO	CO_2	CH_4	C_2H_2	C_2H_4	C_2H_6	C_3+	C_6H_6[b]	H_2/CO
Inlet										
	35.07	17.11	29.65	13.71	0.24	2.66	0.60	0.484	0.495	2.05
At Initial Catalyst Activity										
775	64.05	9.29	25.73	0.76	0.00	0.17	0.00	0.000	0.000	6.90
800	62.93	9.44	26.11	1.52	0.00	0.00	0.00	0.000	0.000	6.70
825	63.75	10.35	25.07	0.66	0.00	0.17	0.00	0.000	0.002	6.15
850	64.14	11.19	23.93	0.57	0.00	0.16	0.00	0.000	0.000	5.75
875	61.38	10.43	27.63	0.41	0.00	0.15	0.00	0.000	0.000	5.60
At Final Catalyst Activity										
775	50.25	13.23	26.72	7.80	0.00	1.45	0.26	0.000	0.282	3.15
800	57.36	11.58	26.41	3.63	0.00	0.00	0.68	0.000	0.122	3.57
825	52.98	13.07	26.02	6.71	0.00	0.97	0.06	0.000	0.190	4.05
850	54.77	12.70	25.68	6.05	0.00	0.69	0.02	0.000	0.084	4.31
875	56.27	12.42	25.49	5.23	0.00	0.50	0.00	0.000	0.084	4.53

[a] Compositions in mol %. [b] Total tars & benzene reported as benzene at inlet (mol %).

Hydrogen sulfide concentration was below the detection level of the MBMS and was not independently measured.

A slipstream (2.7−3.3 slm, including steam) of the volatile product from the TCPDU was introduced into the fluidized-bed reformer (2FBR). Tests were conducted at five temperatures 775, 800, 825, 850, and 875 °C. The inlet molar steam-to-carbon ratio (S/C) was ∼4.5 and the space time was 0.13−0.15 kg h m^{-3}.

In the first phase of every test, a high conversion of tar components and lighter hydrocarbons was observed. This was followed by a period of increasing concentrations because of catalyst deactivation and, finally, by the stabilization of concentrations at a new, higher level. The duration of each test was adjusted to include at least 1 h of operation at the lower-activity pseudo-steady state. To prevent differences in the initial state of the catalyst, a fresh charge of catalyst was used in each experiment.

Table 4 presents reformed gas compositions on a dry, inert gas-free basis. The inlet gas contained approximately 35% hydrogen, 17% carbon monoxide, 30% carbon dioxide, 17% methane, and 0.5% benzene and tars. The inlet gas H_2/CO ratio was 2. At initial activity conditions, the hydrogen concentrations increased to >60%, CO decreased to ∼10%, and methane concentrations decreased to ∼1%. The H_2/CO ratio ranged from 6.9 at 775 °C to 5.6 at 875 °C. At the final pseudo-steady-state condition, hydrogen concentrations were in the mid 50% range, CO ranged from 11.6 to 13.3%, and methane range from 3.6 to 7.8%. The H_2/CO ratio ranged from 3.2 at 775 °C to 4.5 at 875 °C. At the final conditions, the H_2/CO ratio increased with temperature, while at initial activity conditions, the H_2/CO decreased with temperature.

Catalyst Deactivation Kinetics and Model Development. A basic discussion of catalyst deactivation kinetics was presented by Levenspiel[60] in 1979 that included equation derivations, example problems, and sample calculations. The discussion has been updated to include the role of effectiveness factors and a more complete discussion of experimental design.[61] Implicit in the kinetic models developed by Levenspiel is complete catalyst deactivation.

Fuentes[62] showed that the use of general power law equations was only valid when activity declined to zero and proposed the inclusion of a residual steady-state activity. If the activity, a, approaches a residual steady-

Table 5. Kinetic Deactivation Models with Residual Activity (DMRA)

$n = 1$	$n = 2$
$d = 1$	$d = 1$
$k\tau a = \ln\left(\frac{C_{A0}}{C_A}\right)$	$k\tau C_{A0} a = \frac{C_{A0} - C_A}{C_A} = \left(\frac{C_{A0}}{C_A} - 1\right)$
$a = a_{S1} + (1 - a_{S1}) \exp(-\psi^*_{d1} t)$	$a = a_{S1} + (1 - a_{S1}) \exp(-\psi^*_{d1} t)$
$C_A = \frac{C_{A0}}{\exp[k\tau(a_{S1} + (1 - a_{S1}) \exp(-\psi t))]}$	$C_A = \frac{C_{A0}}{1 + k\tau C_{A0}(a_{S1} + (1 - a_{S1}) \exp(-\psi^*_{d1} t))}$
$d = 2$	$d = 2$
$k\tau a = \ln\left(\frac{C_{A0}}{C_A}\right)$	$k\tau C_{A0} a = \frac{C_{A0} - C_A}{C_A} = \left(\frac{C_{A0}}{C_A} - 1\right)$
$a = a_{S2} + \frac{(1 - a_{S2})}{1 + (1 - a_{S2})\psi^*_{d2} t}$	$a = a_{S2} + \frac{(1 - a_{S2})}{1 + (1 - a_{S2})\psi^*_{d2} t}$
$C_A = \frac{C_{A0}}{\exp\left[k\tau\left(a_{S2} + \frac{(1 - a_{S2})}{1 + (1 - a_{S2})\psi^*_{d2} t}\right)\right]}$	$C_A = \frac{C_{A0}}{1 + k\tau C_{A0} a_{S2} + \frac{k\tau C_{A0}(1 - a_{S2})}{1 + (1 - a_{S2})\psi^*_{d2} t}}$
$d = 1$	$d = 1$
$k\tau a = \ln\left[\frac{X_A}{1 - X_A}\right]$	$kt C_{A0} a = \frac{X_A}{1 - X_A}$
$a = a_{S1} + (1 - a_{S1}) \exp(-\psi^*_{d1} t)$	$a = a_{S1} + (1 - a_{S1}) \exp(-\psi^*_{d1} t)$
$X_A = \frac{\exp[k\tau(a_{S1} + (1 - a_{S1}) \exp(^{-\psi t}))]}{1 + \exp[k\tau(a_{S1} + (1 - a_{S1}) \exp(^{-\psi t}))]}$	$X_A = \frac{k\tau C_{A0}(a_{S1} + (1 - a_{S1}) \exp(-\psi t))}{1 + k\tau C_{A0}(a_{S1} + (1 - a_{S1}) \exp(-\psi t))}$

Table 6. Activation Energies

	activation energy	
	k (kJ/g·mol)	ψ (kJ/g·mol)
1st order reaction		
methane-combined	32.0	158.8
methane-GC	21.1	109.3
methane-MBMS	43.7	242.1
ethane	31.5	146.1
benzene	9.3	74.3
tar	18.9	17.9
tar2 (tar + benzene)	45.1	121.2

state activity, a_S, as t approaches infinity, then

$$-\frac{da}{dt} = \psi(C_i, T)(a^d - a_S{}^d) \quad (1)$$

If the deactivation variable is the fraction $(a - a_S)$ of the overall activity that is time dependent, then

$$-\frac{da}{dt} = \psi(C_i, T)(a - a_S)^d \quad (2)$$

Use of the models showed that variations in deactivation order and high deactivation order were, in many cases, mathematical artifacts.

Monzon et al.[63] developed mathematical relationships between the Levenspiel deactivation models and deactivation models with residual activity and showed that use of the Levenspiel model can lead to errors in measuring intrinsic factors such as activation energies when the catalyst maintains a residual activity. They also showed how models with residual activity could be used for comparison and discrimination between kinetic models.

Taralas and Kontominas[41] analyzed the kinetics of toluene destruction over NiMo/γ-Al_2O_3, dolomitic magnesium oxide, quicklime, and calcined dolomite at typical tar-reforming conditions. The influence of hydrogen and water vapor was also studied. A reaction mechanism was proposed and evaluated by a mechanistic Langmuir−Hinshelwood model. Activation energies ranged from 56 to 196 kJ/g·mol, compared to 356 kJ/g·mol for thermal dealkylation.

The objective of the model development was to develop global reaction models for individual compounds converted in the tar-reforming reactor as the first step in developing models that will permit the design of commercial-type catalytic tar-reformer/regenerator systems. It is understood that the rate constants and apparent activation energies resulting from the modeling represent effective constants dependent on the nature of the complex mixture of tar and other species and do not, at this point, represent the fundamental mechanisms. Since the system involves reaction of fluids with a heterogeneous solid catalyst, a number of potential mass transfer steps and chemical reaction steps may be involved. This involved series of steps may be further complicated by noncatalytic, bulk-phase chemical reactions. Levenspiel[61] has summarized the factors influencing reaction rates for heterogeneous reactions.

For a nonporous catalyst where the reactants/products are gases or vapors, the surface reaction becomes the primary rate-influencing factor. In such a case, pore diffusion need not be considered, and simplified reaction kinetic expressions can be expected to provide a reasonable representation of the catalytic chemistry. Because of the low specific surface area and negligible porosity of the NREL catalyst, a simplified model was developed.

The general rate expression for the rate of reaction of a component is

$$-r_A = kC_A{}^n a \quad (3)$$

For a plug-flow reactor, the kinetic rate expression is

$$\frac{W}{V} = \int_0^{X_A} \frac{dX_A}{-r_A} \tag{4}$$

For a constant density system (D = constant), the rate expression defined in terms of space time is

$$\tau = \frac{-1}{kaC_{A0}} \int_{C_{A0}}^{C_A} \frac{dC_A}{C_A{}^n} \tag{5}$$

For the conversion performance indicated by experimental data, a deactivation model with residual activity (DMRA) should better fit the data.

Kinetic expressions were developed for the four combinations of first- and second-order rates for the chemical reaction, eq 5, and catalyst activity, eq 2. The kinetic expressions are shown in Table 5. As discussed later, the initial analysis of the kinetic models, expressed in terms of concentration, showed that the models with a residual activity order of 1 better fit the data than the models with a residual activity order of 2. This was taken into account when developing fractional-conversion models to facilitate the comparison of conversions of different compounds with a wide range of concentrations. Therefore, only fractional-conversion models with first-order activity are presented in Table 5.

Application of Catalyst Deactivation Models To Measured Results. A major goal of investigating the kinetics models was to attempt to differentiate between models based on goodness-of-fit to the data and realism of the estimated catalyst activity and estimated activation energies. The results of an analysis of benzene concentration MBMS data at 825 °C are representative of model fits for first- and second-order reactions and first- and second-order deactivation. SigmaPlot regressions were used to fit the DMRA concentration models given in Table 5. As shown in Figure 4, the DMRA models with first-order deactivation are seen to better fit the experimental data. They better modeled the deactivation period and gave final steady-state concentrations consistent with the data. This is supported by the coefficients of determination for the models. The two models with first-order deactivation had coefficients of determination of 0.954 for first-order kinetics and 0.955 for second-order kinetics. The two models with second-order deactivation had coefficients of determination of 0.915 for first-order kinetics and 0.849 for second-order kinetics.

Figure 5 shows a comparison of benzene-conversion data at five temperatures, expressed as fractional conversion, with the first-order fractional conversion model with first-order deactivation. Only the MBMS data for 775 and 875 °C are shown. Model plots for two experiments at 850 °C indicate the reproducibility of experiments.

Figure 6 presents comparable first-order reaction model results for ethane, using gas chromatograph data. Overall, the model did a very good job of fitting the deactivation data with time and fit the final conversion well. The model did not fit well the initial onset of deactivation at the lower temperatures. Coefficients of determination were in the range of 0.98−0.99. Again, comparable results were obtained for second-order kinetics.

Figure 7 shows a comparison of model results for six components at 825 °C. For clarity, only a portion of the experimental data is shown. With the exception of

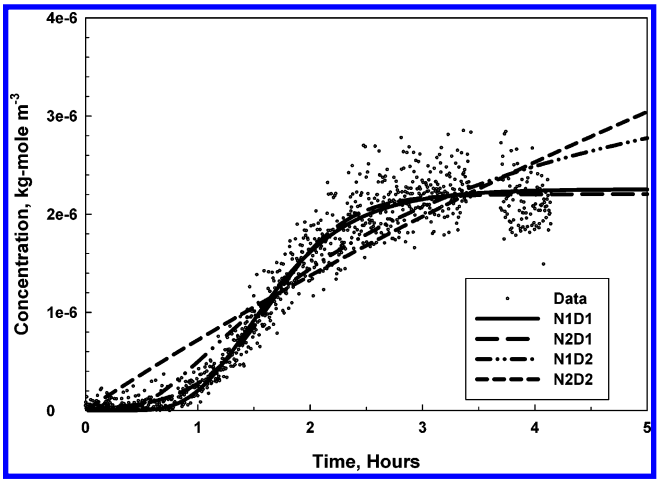

Figure 4. Benzene concentration at 825 °C; comparison of DMRA models.

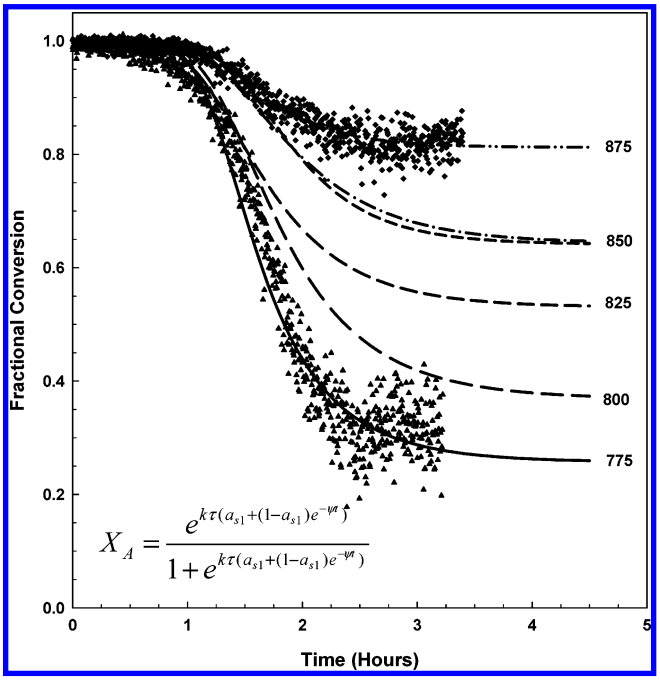

Figure 5. Benzene fractional conversion, first-order reforming kinetics.

methane, all of the components had the same initiation time for the start of deactivation and reached a pseudo-steady-state conversion at the same time. In general, conversions for higher-molecular-weight compounds were higher. The residual total tar (including toluene and naphthalene) conversion at this temperature was 87%.

Table 6 gives activation energies for all the components studied using the first-order kinetic model. In general, the activation-energy values are reasonable. Exceptions are those for naphthalene, which had a negative value for the first-order rate constant, and toluene, which had a negative value for the deactivation rate constant. In both cases, there were apparent inconsistencies in the deactivation data for one temperature. The deactivation reaction activation energy for benzene was 74.3 kJ/g·mol. For tar, the apparent activation energies were 18.9 kJ/g·mol for reforming and 17.9 kJ/g·mol for deactivation. The tar values are empirical since they represent an average of all tar compounds and will vary as tar composition changes. For comparison purposes, a second empirical tar was

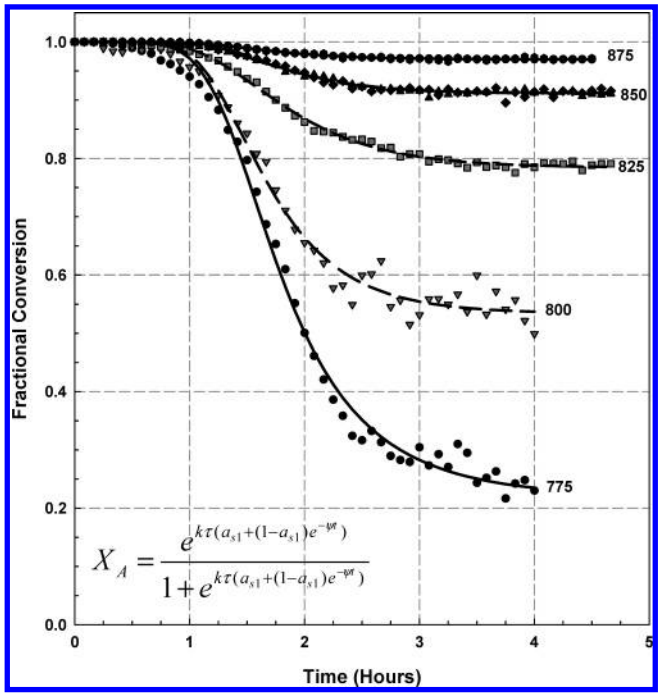

Figure 6. Ethane fractional conversion, first-order reforming kinetics.

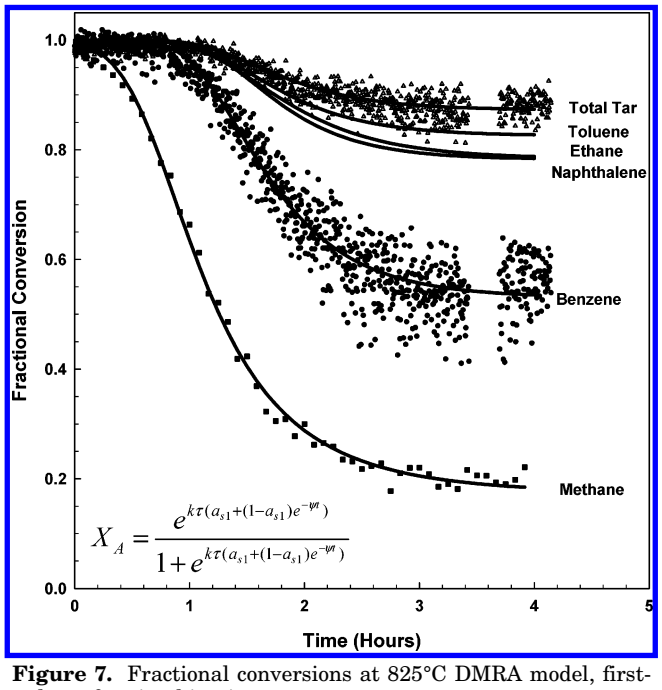

Figure 7. Fractional conversions at 825°C DMRA model, first-order reforming kinetics.

defined that included benzene (tar2) for comparison to previous studies whose definition of tar included benzene. For tar2, the apparent reforming activation energy was 45.1 kJ/g·mol and the apparent deactivation activation energy was 121.2 kJ/g·mol. Comparable literature tar2 reforming activation energies are 30−50 kJ g·mol[24] for reforming catalysts, 72 kJ/g·mol for a nickel steam methane-reforming catalyst,[25] and 84−100 for calcined dolomite.[13,14]

The first-order kinetic constants for methane demonstrate the sensitivity of the estimated activation energy to small differences in data. The combined data, Table 6, gave an activation energy of 32 kJ/g·mol for the first-order reforming rate constant, while the model

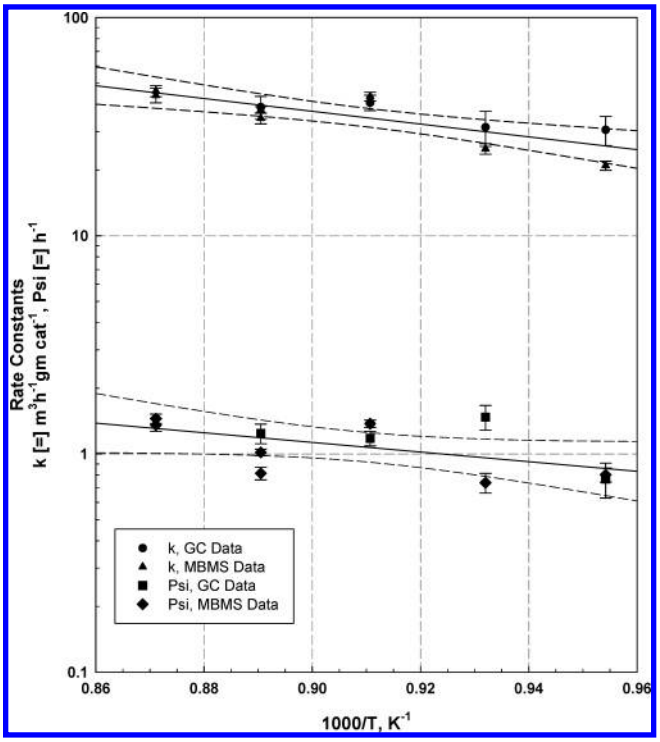

Figure 8. First-order Arrhenius plot for methane using both GC and MBMS Data.

based on GC data alone gave an activation energy of 21.1 kJ/g·mol, and that based on the MBMS data alone gave an activation energy of 43.7 kJ/g·mol. The error bars represent ±2 standard errors for the parameter. For the deactivation rate constant, the combined activation energy was 158.8 kJ/g·mol, for the model based on GC data it was 109.3 kJ/g·mol, and for the model based on MBMS data it was 242.1 kJ/g·mol. Twigg[64] gave values of activation energy for classical methane reforming of 77 kJ/g·mol at 800−900 °C and 100 kJ/g·mol at 700−800 °C, and Bartholomew[65] presented catalyst-sintering activation energies for nickel catalysts ranging from 32 to 159 kJ/g·mol. Taralas and Kontominas[41] estimated activation energies for catalytic reforming of toluene from 56 kJ/g·mol (Ni catalyst) to 196 kJ/g·mol (calcined quicklime). Simell et al.[66] estimated activation energies for benzene decomposition over a dolomite catalyst as 125−182 kJ/g·mol for various kinetic models.

The data were also analyzed using second-order reforming kinetics with first-order deactivation. The second-order model gave values of activation energies from 8.4 kJ/g·mol for naphthalene to 28.8 kJ/g·mol for ethane. However, except for methane, the model gave negative activation energies for the deactivation rate constant. For methane, the catalyst deactivation rate constant was 5.8 kJ/g·mol. Although the second-order reforming kinetics model adequately fits the data, the first-order model provides a more realistic estimate of activation energies (see Figure 8 for first-order model results).

Figure 9 gives the experimental residual fractional conversion after catalyst deactivation for all components as a function of temperature. The regression lines represent a simple least-squares fit of the data. Higher conversions were seen for the heavier tar components than for lighter components such as benzene, ethane, and methane. At 875°C, the conversion of tar and

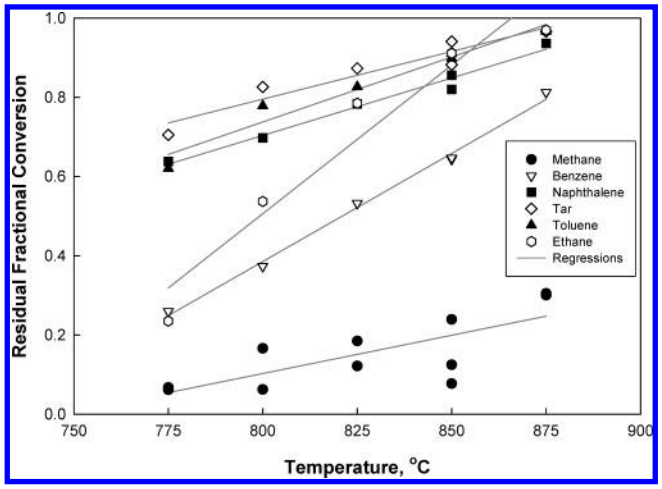

Figure 9. Residual fractional conversions.

toluene were 97% and the conversion of naphthalene was 94%. Benzene conversion was also relatively high, 80%.

Conclusions

In this study, an evaluation of the kinetics of tar and other hydrocarbon-reforming global kinetics using biomass-derived syngas was performed with the goal of incorporating the level of detail normally seen in model compound studies. This was successfully accomplished using a pilot gasification system coupled to a bench-scale reforming system with on-line material balances and on-line comprehensive measurements of gas compositions and selected tar compounds.

Results of the kinetic evaluation of the reforming data show that deactivation models with residual activities can adequately model the initial deactivation of a selected tar-reforming catalyst. First-order deactivation kinetics models better fit the data than do second-order deactivation models. Both first-order and second-order reforming kinetic models fit the data, but activation energy results indicate that first-order kinetics provide more realistic estimates for most components. More detailed mechanistic models, including other components and other reactions such as the water gas shift reaction are needed to provide confidence that reactions are being correctly interpreted.

Acknowledgment

The authors thank the U.S. Department of Energy, Office of the Biomass Program, for financial support provided through DOE Subcontract DE-AC36-99GO10337.

Nomenclature

a = catalyst activity factor
a_{S1} = residual catalyst activity
A = component of interest
C = concentration, g·mole/L or kg·mole/m^3
d = order of deactivation
E_a = apparent activation energy, kJ/g·mole
k = rate constant: first order [=] m^3 h^{-1} kg cat^{-1}; second order [=] (m^3 kg cat^{-1} h^{-1})(m^3 kg mole^{-1})
n = reaction order
n' = order of concentration dependency of deactivation
P = poison
r = rate of reaction of A
R = product of reaction of A
t = time, hours
Ψ = deactivation rate constant (severity factor), h^{-1}
τ = weight time, kg h m^{-3}

Literature Cited

(1) French, R. J.; Czernik, S. Hydrogen production by steam reforming of waste vegetable oils. *Abstr. Pap. Am. Chem. Soc.* **2003**, *226*, U536−U536.

(2) Evans, R. J.; Chornet, E.; Czernik, S.; Feik, C.; French, R.; Phillips, S.; Yeboah, Y. D.; Day, D.; Ellis, S.; McGee, D.; Realff, M. J. Hydrogen from biomass by catalytic steam reforming of biomass pyrolysis vapors. *Abstr. Pap. Am. Chem. Soc.* **2003**, *226*, U536−U536.

(3) Hos, J. J.; Groeneveld, M. J. Biomass Gasification. In *Biomass*; Hall, D. O., Overend, R. P., Eds.; Wiley and Sons: Chichester, U.K., 1987; pp 237−255.

(4) Beenackers, A. A. C. M.; van Swaaij, W. P. M. Gasification of Biomass: A State of the Art Review. In *Thermochemical Processing of Biomass*; Bridgwater, A. V., Ed.; Butterworth: London, U.K., 1984; pp 91−136.

(5) Narvaez, I.; Orio, A.; Aznar, M. P.; Corella, J. Biomass gasification with air in an atmospheric bubbling fluidized bed. Effect of six operational variables on the quality of the produced raw gas. *Ind. Eng. Chem. Res.* **1996**, *35* (7), 2110−2120.

(6) Dayton, D. C. *Review of the Literature on Catalytic Biomass Tar Destruction: Milestone Completion Report*; Report TP-510-32815; National Renewable Energy Laboratory: Golden, CO, 2002; p 33.

(7) Abu El-Rub, Z.; Bramer, E. A.; Brem, G. Review of catalysts for tar elimination in Biomass gasification processes. *Ind. Eng. Chem. Res.* **2004**, *43* (22), 6911−6919.

(8) Sutton, D.; Kelleher, B.; Ross, J. R. H. Review of literature on catalysts for biomass gasification. *Fuel Process. Technol.* **2001**, *73* (3), 155−173.

(9) Simell, P.; Kurkela, E.; Stahlberg, P.; Hepola, J. Catalytic hot gas cleaning of gasification gas. *Catal. Today* **1996**, *27* (1−2), 55−62.

(10) Vassilatos, V.; Taralas, G.; Sjostrom, K.; Bjornbom, E. Catalytic Cracking of Tar in Biomass Pyrolysis-Gas in the Presence of Calcined Dolomite. *Can. J. Chem. Eng.* **1992**, *70* (5), 1008−1013.

(11) Taralas, G. Catalytic steam pyrolysis of a selected saturated hydrocarbon on calcined mineral particles. *Can. J. Chem. Eng.* **1998**, *76* (6), 1093−1101.

(12) Perez, P.; Aznar, P. M.; Caballero, M. A.; Gil, J.; Martin, J. A.; Corella, J. Hot gas cleaning and upgrading with a calcined dolomite located downstream a biomass fluidized bed gasifier operating with steam−oxygen mixtures. *Energy Fuels* **1997**, *11* (6), 1194−1203.

(13) Orio, A.; Corella, J.; Narvaez, I. Performance of different dolomites on hot raw gas cleaning from biomass gasification with air. *Ind. Eng. Chem. Res.* **1997**, *36* (9), 3800−3808.

(14) Delgado, J.; Aznar, M. P.; Corella, J. Biomass gasification with steam in fluidized bed: Effectiveness of CaO, MgO, and CaO−MgO for hot raw gas cleaning. *Ind. Eng. Chem. Res.* **1997**, 36 (5), 1535−1543

(15) Delgado, J.; Aznar, M. P.; Corella, J. Calcined dolomite, magnesite, and calcite for cleaning hot gas from a fluidized bed biomass gasifier with steam: Life and usefulness. *Ind. Eng. Chem. Res.* **1996**, *35* (10), 3637−3643.

(16) Corella, J.; Aznar, M. P.; Gil, J.; Caballero, M. A. Biomass gasification in fluidized bed: Where to locate the dolomite to improve gasification? *Energy Fuels* **1999**, *13* (6), 1122−1127.

(17) Corella, J.; Toledo, J. M.; Padilla, R. Olivine or dolomite as in-bed additive in biomass gasification with air in a fluidized bed: Which is better? *Energy Fuels* **2004**, *18* (3), 713−720.

(18) Gil, J.; Caballero, M. A.; Martin, J. A.; Aznar, M. P.; Corella, J. Biomass gasification with air in a fluidized bed: Effect of the in-bed use of dolomite under different operation conditions. *Ind. Eng. Chem. Res.* **1999**, *38* (11), 4226−4235.

(19) Olivares, A.; Aznar, M. P.; Caballero, M. A.; Gil, J.; Frances, E.; Corella, J. Biomass gasification: Produced gas upgrading by in-bed use of dolomite. *Ind. Eng. Chem. Res.* **1997**, *36* (12), 5220−5226.

(20) Aznar, M. P.; Corella, J.; Delgado, J.; Lahoz, J. Q. Improved Steam Gasification of Lignocellulosic Residues in a Fluidized-Bed with Commercial Steam Reforming Catalysts. *Ind. Eng. Chem. Res.* **1993**, *32* (1), 1−10.

(21) Aznar, M. P.; Caballero, M. A.; Gil, J.; Martin, J. A.; Corella, J. Commercial Steam Reforming Catalysts To Improve Biomass Gasification with Steam−Oxygen Mixtures. 2. Catalytic Tar Removal. *Ind. Eng. Chem. Res.* **1998**, *37* (7), 2668−2680.

(22) Caballero, M. A.; Aznar, M. P.; Gil, J.; Martin, J. A.; Frances, E.; Corella, J. Commercial steam reforming catalysts to improve biomass gasification with steam−oxygen mixtures. 1. Hot gas upgrading by the catalytic reactor. *Ind. Eng. Chem. Res.* **1997**, *36* (12), 5227−5239.

(23) Caballero, M. A.; Corella, J.; Aznar, M. P.; Gil, J. Biomass gasification with air in fluidized bed. Hot gas cleanup with selected commercial and full-size nickel-based catalysts. *Ind. Eng. Chem. Res.* **2000**, *39* (5), 1143−1154.

(24) Corella, J.; Orio, A.; Toledo, J. M. Biomass gasification with air in a fluidized bed: Exhaustive tar elimination with commercial steam reforming catalysts. *Energy Fuels* **1999**, *13* (3), 702−709.

(25) Narvaez, I.; Corella, J.; Orio, A. Fresh tar (from a biomass gasifier) elimination over a commercial steam-reformimg catalyst. Kinetics and effect of different variables of operation. *Ind. Eng. Chem. Res.* **1997**, *36* (2), 317−327.

(26) Sutton, D.; Kelleher, B.; Doyle, A.; Ross, J. R. H. Investigation of nickel supported catalysts for the upgrading of brown peat derived gasification products. *Bioresour. Technol.* **2001**, *80* (2), 111−116.

(27) Corella, J.; Orio, A.; Aznar, P. Biomass gasification with air in fluidized bed: Reforming of the gas composition with commercial steam reforming catalysts. *Ind. Eng. Chem. Res.* **1998**, *37* (12), 4617−4624.

(28) Darvell, L. I.; Heiskanen, K.; Jones, J. M.; Ross, A. B.; Simell, P.; Williams, A. An investigation of alumina-supported catalysts for the selective catalytic oxidation of ammonia in biomass gasification. *Catal. Today* **2003**, *81* (4), 681−692.

(29) Leppalahti, J.; Simell, P.; Kurkela, E. Catalytic Conversion of Nitrogen-Compounds in Gasification Gas. *Fuel Process. Technol.* **1991**, *29* (1−2), 43−56.

(30) Wang, W.; Padban, N.; Ye, Z.; Andersson, A.; Bjerle, I. Kinetics of Ammonia Decomposition in Hot Gas Cleaning. *Ind. Eng. Chem. Res.* **1999**, 38 (11), 4175−4182.

(31) Corella, J.; Aznar, M. P.; Delgado, J.; Martinez, M. P.; Aragues, J. L. Deactivation of tar cracking stones (dolomites, calcites, magnesites) and of commercial methane steam reforming catalysts in the upgrading of the exit gas from steam fluidized bed gasifiers of biomass and organic wastes. *Stud. Surf. Sci. Catal.* **1991**, *68*, 249−252.

(32) Hepola, J.; Simell, P.; Kurkela, E.; Stahlberg, P. Sulfur Poisoning of Nickel-Catalysts in Catalytic Hot Gas Cleaning Conditions of Biomass Gasification. *Catal. Deact. 1994, Proc. Int. Symp., 6th* **1994**, *88*, 499−506.

(33) Hepola, J.; Simell, P. Sulphur poisoning of nickel-based hot gas cleaning catalysts in synthetic gasification gas. I. Effect of different process parameters. *Appl. Catal., B* **1997**, *14* (3−4), 287−303.

(34) Hepola, J.; Simell, P. Sulphur poisoning of nickel-based hot gas cleaning catalysts in synthetic gasification gas. II. Chemisorption of hydrogen sulphide. *Appl. Catal., B* **1997**, 14 (3−4), 305−321.

(35) Hepola, J.; Simell, P. Sulfur poisoning of nickel-based hot gas cleaning catalysts in synthetic gasification gas. *Catal. Deact. 1997, Proc. Int. Symp., 7th* **1997**, *111*, 471−478.

(36) Bangala, D. N.; Abatzoglou, N.; Chornet, E. Steam reforming of naphthalene on Ni−Cr/Al2O3 catalysts doped with MgO, TiO_2, and La_2O_3. *AIChE J.* **1998**, *44* (4), 927−936.

(37) Bangala, D. N.; Abatzoglou, N.; Martin, J. P.; Chornet, E. Catalytic gas conditioning: Application to biomass and waste gasification. *Ind. Eng. Chem. Res.* **1997**, *36* (10), 4184−4192.

(38) Depner, H.; Jess, A. Kinetics of nickel-catalyzed purification of tarry fuel gases from gasification and pyrolysis of solid fuels. *Fuel* **1999,** *78* (12), 1369−1377.

(39) Coll, R.; Salvado, J.; Farriol, X.; Montane, D. Steam reforming model compounds of biomass gasification tars: Conversion at different operating conditions and tendency towards coke formation. *Fuel Process. Technol.* **2001,** *74* (1), 19−31.

(40) Wang, D.; Czernik, S.; Montane, D.; Mann, M.; Chornet, E. Biomass to hydrogen via fast pyrolysis and catalytic steam reforming of the pyrolysis oil or its fractions. *Ind. Eng. Chem. Res.* **1997**, *36* (5), 1507−1518.

(41) Taralas, G.; Kontominas, M. G. Kinetic modelling of VOC catalytic steam pyrolysis for tar abatement phenomena in gasification/pyrolysis technologies. *Fuel* **2004**, *83*, (*9*), 1*235*−1245.

(42) Bartholomew, C. H. Mechanisms of catalyst deactivation. *Appl. Catal., A* **2001**, *212* (1−2), 17−60.

(43) Mleczko, L. S. M.; Wurzel, T. Catalytic reformer−combustor: A novel reactor concept for synthesis gas production. *Ind. Eng. Chem. Res.* **1997**, *36*, 4459−4465.

(44) Garcia, L.; French, R.; Czernik, S.; Chornet, E. Catalytic steam reforming of bio-oils for the production of hydrogen: Effects of catalyst composition. *Appl. Catal., A* **2000**, *201* (2), 225−239.

(45) Baker, E. G.; Mudge, L. K. Mechanisms of Catalytic Biomass Gasification. *J. Anal. Appl. Pyrolysis* **1984**, *6* (3), 285−297.

(46) Baker, E. G.; Mudge, L. K.; Brown, M. D. Steam Gasification of Biomass with Nickel Secondary Catalysts. *Ind. Eng. Chem. Res.* **1987**, 26 (7), 1335−1339.

(47) Brown, M. D.; Mudge, L. K.; Baker, E. G. Catalysts for Gasification of Biomass. *Biotechnol. Bioeng.* **1984**, 125−136.

(48) Mitchell, D. H.; Mudge, L. K.; Robertus, R. J.; Weber, S. L.; Sealock, L. J. Gasohol−Biomass Developments−Methane−Methanol by Catalytic Gasification of Biomass. *Chem. Eng. Prog.* **1980**, *76* (9), 53−57.

(49) Mudge, L. K.; Baker, E. G.; Mitchell, D. H.; Brown, M. D. Catalytic Steam Gasification of Biomass for Methanol and Methane Production. *J. Sol. Energy Eng.* **1985**, *107* (1), 88−92.

(50) Corella, J.; Adanez, J.; Monzon, A. Some Intrinsic Kinetic Equations and Deactivation Mechanisms Leading to Deactivation Curves with a Residual Activity. *Ind. Eng. Chem. Res.* **1988**, *27* (3), 375−381.

(51) Corella, J.; Toledo, J. M.; Aznar, M. P. Improving the modeling of the kinetics of the catalytic tar elimination in biomass gasification. *Ind. Eng. Chem. Res.* **2002**, *41* (14), 3351−3356.

(52) Corella, J.; Caballero, M. A.; Aznar, M. P.; Brage, C. Two advanced models for the kinetics of the variation of the tar composition in its catalytic elimination in biomass gasification. *Ind. Eng. Chem. Res.* **2003**, *42* (13), 3001−3011.

(53) Corella, J.; Monzon, A. Modeling of the Deactivation Kinetics of Solid Catalysts by Two or More Simultaneous and Different Causes. *Ind. Eng. Chem. Res.* **1988**, *27* (3), 369−374.

(54) French, R. J.; Magrini-Bair, K. A.; Czernik, S.; Parent, Y.; Chornet, E. Fluidizable catalysts for hydrogen production by steam reforming of biomass pyrolysis products. *Abstr. Pap. Am. Chem. Soc.* **2002**, *224*, U579−U579.

(55) Garcia, L.; French, R.; Czernik, S.; Chornet, E. Catalytic steam reforming of bio-oils for the production of hydrogen: Effects of catalyst composition. *Appl. Catal., A* **2000**, *201* (2), 225−239.

(56) Brown, A. L.; Dayton, D. C.; Nimlos, M. R.; Daily, J. W. Design and Characterization of an Entrained Flow Reactor for the Study of Biomass Pyrolysis Chemistry at High Heating Rates. *Energy Fuels* **2001**, *15* (5), 1276−1285.

(57) Dayton, D. C.; French, R. J.; Milne, T. A. Direct Observation of Alkali Vapor Release during Biomass Combustion and Gasification. 1. Application of Molecular Beam/Mass Spectrometry to Switchgrass Combustion. *Energy Fuels* **1995**, *9* (5), 855−65.

(58) Evans, R. J.; Milne, T. A. Molecular Characterization of the Pyrolysis of Biomass. 2. Applications. *Energy Fuels* **1987**, *1* (4), 311−319.

(59) Evans, R. J.; Milne, T. A. Molecular Characterization of the Pyrolysis of Biomass. 1. Fundamentals. *Energy Fuels* **1987**, *1* (2), 123−137.

(60) Levenspiel, O. *The Chemical Reactor Omnibook*; OSU Book Stores, Inc.: Corvalis, OR, 1979.

(61) Levenspiel, O. *Chemical Reaction Engineering*, 3rd ed.; John Wiley & Sons: Hoboken, NJ, 1999; p 668.

(62) Fuentes, G. A. Catalyst Deactivation and Steady-State Activity−A Generalized Power-Law Equation Model. *Appl. Catal.* **1985**, *15* (1), 33−40.

(63) Monzon, A., Romeo, E., Borgna, A. Relationship between the kinetic parameters of different catalyst deactivation models. *Chem. Eng. J.* **2003**, *94* (1), 19−28.

(64) Twigg, M. V. *Catalyst Handbook*, 2nd ed.; John Wiley & Sons: Hoboken NJ, 1995.

(65) Bartholomew, C. H. Sintering Kinetics of Supported Metals—New Perspectives from a Unifying GPLE Treatment. *Appl. Catal., A* **1993**, *107* (1), 1−57.

(66) Simell, P. A.; Hakala, N. A. K.; Haario, H. E.; Krause, A. O. I. Catalytic decomposition of gasification gas tar with benzene as the model compound. *Ind. Eng. Chem. Res.* **1997**, *36* (1), 42−51.

Received for review January 24, 2005
Revised manuscript received July 7, 2005
Accepted August 5, 2005

IE050098W